Published in final edited form as:
J Biomech. 2007 ; 40(8): 1676–1685.

Effects of Implant Design Parameters on Fluid Convection, Potentiating 3rd Body Debris Ingress into the Bearing Surface during THA Impingement/Subluxation

Hannah J. Lundberg[*,†], **Douglas R. Pedersen**[*,†], **Thomas E. Baer**[*], **Marian Muste**[‡], **John J. Callaghan**[*,†], and **Thomas D. Brown**[*,†]

***** *Department of Orthopaedics and Rehabilitation, University of Iowa, Iowa City IA 52242*

† *Department of Biomedical Engineering, University of Iowa, Iowa City IA 52242*

‡ *Department of IIHR-Hydroscience and Engineering, University of Iowa, Iowa City IA 52242*

Abstract

Aseptic loosening from polyethylene wear debris is the leading cause of failure for metal-on-polyethylene total hip implants. Third body debris ingress to the bearing space results in femoral head roughening and acceleration of polyethylene wear. How third body particles manage to enter the bearing space between the closely conforming articulating surfaces of the joint is not well understood. We hypothesize that one such mechanism is from convective fluid transport during subluxation of the total hip joint. To test this hypothesis, a three-dimensional computational fluid dynamics model was developed and validated, to quantify fluid ingress into the bearing space during a leg-cross subluxation event. The results indicated that extra-articular joint fluid could be drawn nearly to the pole of the cup with even very small separations of the femoral head (<0.60 mm). Debris suspended near the equator of the cup at the site of maximum fluid velocity just before the subluxation began could be transported to within 11° from the cup pole. Larger head diameters resulted in increased fluid velocity at all sites around the entrance to the gap compared to smaller head sizes, with fluid velocity being greatest along the anterosuperolateral cup edge, for all head sizes. Fluid pathlines indicated that suspended debris would reach similar angular positions in the bearing space regardless of head size. Increased inset of the femoral head into the acetabular cup resulted both in higher fluid velocity and in transport of third body debris further into the bearing space.

Keywords

wear; third body; total hip arthroplasty; computational model

INTRODUCTION

Aseptic loosening from polyethylene wear debris is the leading cause of failure for metal-on-polyethylene total hip implants (Dowd et al., 2000;Dumbleton et al., 2002). Specific subsets

Corresponding Author: Thomas D. Brown, Ph.D., Orthopaedic Biomechanics Laboratory, 2181 Westlawn, University of Iowa, Iowa City, IA 52242, tom-brown@uiowa.edu, (319) 335-7528, Fax (319) 335-7530

Review overseen by: J.J. Trey Crisco, Ph.D., Professor and Director, Bioengineering Laboratory, Department of Orthopaedics, Brown Medical School/Rhode Island Hospital

of patients within any given similarly implanted cohort tend to experience pronounced wear rate acceleration compared to group norms. These outlier patients are the ones most susceptible to early implant failure from aseptic loosening (Dowd et al., 2000). Third body debris ingress into the joint is one suspected culprit for outlier wear, because it results in roughening of the metal femoral head, dramatically increasing polyethylene wear. The presence of third body particles embedded in the polyethylene surface and in surrounding tissues is a well-documented finding at revision surgery. Third body and polyethylene particles are present in the joint fluid and peri-articular tissues, but it is unknown how they enter the bearing space between the closely conforming articulating surfaces of the bearing.

A potential mechanism for third body ingress is via convective fluid ingress during bearing space separation. Fluoroscopic recordings during the swing phase of gait (Komistek et al., 2002) have shown an average of 2 mm of separation. Other work has shown an average separation of 1.2 mm during gait and 2.4 mm during leg lift (Lombardi et al., 2000). Separation between the femoral head and acetabular cup also occurs during impingement-induced lever-out subluxation of the hip, a precursor to dislocation. Prevalence of impingement damage in retrieved implants (indicative of subluxation) typically varies from about 40 to 65% (Hall et al., 1998;Jasty et al., 1997;Shon et al., 2005;Yamaguchi et al., 2000;Yamaguchi et al., 1999).

To test the hypothesis that convective fluid transport during subluxation provides a particle ingress mechanism, a three-dimensional computational fluid dynamics (CFD) model was developed. The specific subluxation event modeled was leg-cross subluxation. The model's paradigm was that fluid motion would govern the transport of fluid-suspended third body particles into the bearing space. A two-dimensional validation was performed against a corresponding experiment using particle image velocimetry (PIV). The full 3D CFD model of leg-cross subluxation was parametrically exercised to determine the effects of implant design parameters on fluid ingress.

METHODS

The mesh for the 3D CFD model was generated using Truegrid v2.1.5 (XYZ Scientific Applications, Inc., Livermore, CA). Navier-Stokes equation solutions were obtained using ADINA-F v8.2 (ADINA R&D, Inc., Watertown, MA). The model consisted of 93,825 8-noded hexahedral fluid elements. The region of interest was the capsule-enclosed region of the joint space, plus the (thin) bearing space between the femoral head and acetabulum (Figure 1).

Subluxation kinematics for femoral head movement were taken from a finite element (FE) model of leg-cross dislocation (Nadzadi et al., 2002). The CFD simulation started at the instant of initiation of femoral neck impingement, and continued for an additional 0.012 seconds, corresponding to the early subluxation phase of the overall Nadzadi et al. dislocation simulation (Figure 2, Table 1).

The initial fluid mesh elements overlapped near the femoral head as the head displaced and rotated. To deal with this issue, "mapping files" were created in ADINA-F, and successively applied as needed to remesh new models. The mapping files contained nodal pressure, velocity, and position information, as well as element connectivity. Whenever the model could not solve due to fluid mesh overlap, a new CFD mesh was created, and the mapping file from the last successful solution increment of the previous model was applied as initial conditions for the new CFD mesh. UNIX shell scripts and Gawk programs were used to automate this procedure.

Convergence tests of the CFD mesh were performed for three different directions along the gap between the acetabular cup and femoral head: across the gap thickness, along a meridional line from the equator to the pole of the acetabular cup through the coronal plane, and along the equator of the acetabular cup. Convergent mesh refinement involved 25,600 elements in the

bearing space fluid layer between the femoral head and acetabular surface. Elements along the femoral head surface were assigned mesh biasing, resulting in a finer mesh near the entrance to the gap, and a coarser mesh inferiorly on the femoral head surface and towards the pole of the acetabular cup. The external boundaries of the CFD mesh were taken from the internal geometry of the hip capsule (Stewart et al., 2004).

A parametric study was conducted to investigate the effects of variations in six implant design parameters on fluid ingress velocity (Figure 1C): femoral head diameter, bevel angle and face width of the chamfer, initial thickness of the gap between the femoral head and acetabulum, head inset, and fluid viscosity. The baseline case consisted of a 28 mm femoral head diameter, with a 0.1 mm gap between the femoral head and acetabular component, with a chamfer spanning 25% of the polyethylene liner thickness at an angle of 30°, with 0 mm of head inset, and fluid viscosity of 1 Pa-s (Table 2). For the fluid viscosity series, a case of non-Newtonian fluid viscosity was implemented in terms of a shear-thinning fluid whose constitutive coefficients were fitted to a simplified Cross model as reported by Mazzucco et al. (2004).

Fluid pathlines were calculated to determine sites to which suspended third body particles could potentially be transported during leg-cross subluxation. Pathlines were calculated by integrating velocity solutions, using fourth order Runge-Kutta numerical integration in Matlab (The Mathworks, Inc., Natick, MA).

For validation, results from a 2D analog of the CFD model (Figure 3) were compared to a corresponding 2D experimental model. The 2D model initiated with a 0.1 mm gap between the femoral head (28 mm diameter) and acetabular cup. The fluid was assumed to be Newtonian and incompressible. The viscosity was set equal to the viscosity of water (0.001 Pa-s), for comparison with the 2D experimental model in which water was used. The 2D model was composed entirely of three-noded triangular elements. The femoral head was designated as a rigid moving boundary (also “no slip”), and was moved (subluxed/separated) out of the cup at a speed of 0.5 mm/s. Parametric exercise of the 2D model was performed to determine the effect of the size of the gap (0.1 to 0.00001 mm) between the femoral head and acetabular cup on fluid velocity.

For the physical model (Figure 3), PIV was used to measure fluid velocity during a 2D analog of femoral head subluxation. Neutrally buoyant marker particles (100m diameter) suspended in the fluid were illuminated with two halogen lights, through clear slits in the otherwise opaque sides of the device. Particle movement was recorded with a digital video camera (Sony DCR-VX2000). Image processing with EdPIV® software was used to track particle movement and calculate fluid velocity. The PIV fluid velocities were then compared to corresponding fluid velocity fields from the 2D CFD model.

RESULTS

Leg-cross subluxation resulted in very high fluid ingress velocities along the entrance to the articulation gap (maximum 5929 mm/second initial fluid velocity for a 28 mm head, ~120 times the velocity of head movement) (Figure 4). The magnitude of fluid ingress velocity was greatest at the anterosuperolateral cup edge and decreased toward the pole of the cup. From the time of initial subluxation until 0.010 seconds, the fluid ingress velocity magnitude gradually decreased (Figure 5). Beginning at 0.011 seconds, there was a sharp increase in fluid velocity at all ingress points along the entrance to the gap between the head and cup, concomitant with the abrupt change in direction of head motion shown in Figure 2. Subsequently, fluid velocity continued to increase slightly, especially in the region near that of maximum ingress velocity magnitude. This region remained the site of maximum fluid ingress velocity throughout the entire subluxation event.

Fluid pathlines showed that suspended third body particles initiating at the site of maximum ingress velocity could potentially be drawn to within 11° of the pole of the acetabular cup (Figure 6). The example pathline in Figure 6A shows the movement for fluid (or a suspended particle) starting at point (1), just outside the entrance to the gap between the head and the cup, at the beginning of the subluxation. Each dot along the pathline shows the location for the particle at successive time-steps. The example pathline in Figure 6B shows the movement for fluid starting later (time = 0.011 seconds) from that same point. In this case, fluid could be drawn only to within 67.4° of the pole. If the subluxation was continued to 0.015 seconds, third body particles from the site of maximum entrance velocity could be carried past the pole of the acetabular cup. However, there was also a substantial area of the cup still "unreachable" by third body debris (Figure 6C).

Neither chamfer angle nor chamfer thickness had an appreciable effect on fluid velocity. However, fluid velocity magnitude consistently increased when the femoral head diameter increased (Figure 7). For all five head sizes (22, 28, 32, 36, and 40 mm), the maximum velocity magnitude along a circumferential line at the equator of the femoral head was consistently located anterosuperolaterally. The time-wise progression of fluid ingress velocity magnitude was also similar for the five head sizes, tending to decrease from its initial maximum until 0.010 seconds, again followed by a sharp increase beginning at 0.011 seconds, after which time velocity continued to increase slightly. Pathlines were compared for all five head sizes. As reported above, the 28 mm femoral head diameter subluxation case could draw suspended debris from the maximum-velocity site just outside the entrance of the gap to 11.0° away from the pole of the acetabular cup. Similarly, for 22, 32, 36, and 40 mm femoral head diameters, particles starting at the same point along the equator of the femoral head could be drawn to within 11.6°, 13.6°, 11.8°, and 11.8° of the pole of the acetabular cup, respectively.

Fluid velocity magnitude decreased when the width of the initial gap between the femoral head and acetabular cup was increased. The maximum velocity magnitude for all three gap widths (0.05, 0.1, and 0.2 mm) along a circumferential line at the equator of the femoral head was again located anterosuperolaterally. Solutions for the gap width of 0.05 mm could be obtained only for the first 0.007 seconds. (Past 0.007 seconds, there was fluid mesh closure where contact would have occurred between the acetabular cup and the femoral head.) Fluid pathlines showed that fluid starting at the same point along the equator of the femoral head could be drawn to within 7.8°, 24.4°, and 43.5° of the pole after 0.007 seconds for gap widths of 0.05, 0.10, and 0.20 mm, respectively. After 0.012 seconds (the end of the subluxation), fluid from that site could be drawn to within 11.0° and 23.7° of the pole of the acetabular cup for gap widths of 0.10 and 0.20 mm, respectively.

For the head inset series, the velocity progression was different than for the head size series (Figure 8). For a +2 mm head inset, velocity magnitude increased sharply from the onset of the subluxation. Conversely, velocity magnitude decreased from the onset of the subluxation for a −2 mm head inset. Compared to baseline (0 mm inset), overall velocity magnitude was also much greater for +2 mm head inset, and much less for −2 mm head inset. (Solutions for the +2 mm head inset could only be obtained to 0.008 seconds, again because of fluid mesh closure at the site of close proximity of the femoral head and acetabular cup.)

Particle traces of potential areas of third body particle suspension in the joint fluid showed that after 0.008 seconds, debris from the maximum-velocity site could be transported to within 19.7° of the pole of the acetabular cup for the +2 mm head inset. This debris necessarily traveled through a greater arc length than if there was a 0 mm head inset (38.5° versus 30.1°), owing to the greater head coverage. For head inset of 0 mm, corresponding debris could reach to within 19.9° of the pole of the acetabular cup after 0.008 seconds. For −2 mm of head inset, the cup covered less (41.8%) of the total femoral head surface area than for the +2 or 0 mm

head inset models. However, for −2 mm inset, debris from the maximum-velocity ingress site could only be transported to within 31° of the pole after 0.008 seconds. The arc length through which debris could move for a head inset of −2 mm was only 10.8°, appreciably less than that of a cup with a head inset of 0 mm (19°) or +2 mm (38.5°). Particle traces for the model with −2 mm of head inset also showed that even after 0.012 seconds (the end of the subluxation), corresponding debris still could only reach a site 31° away from the pole.

Increasing the fluid viscosity by 3 orders of magnitude did not cause noticeable change in fluid velocity magnitude. However, decreasing the fluid viscosity by 3 orders of magnitude resulted in decreased peak fluid velocity magnitude throughout the subluxation. Fluid peak velocity magnitude for the non-Newtonian fluid viscosity case also showed decrease very similar to that for the decreased fluid viscosity results. After 0.011 seconds, the time point when there was a jump in fluid velocity, the velocity distribution changed for the decreased and non-Newtonian viscosity models, becoming more uniform circumferentially around the equator of the femoral head. Fluid initially just outside the gap entrance could reach 37.9°, 11°, 11.6°, and 13.6° from the pole after 0.012 seconds, for the decreased, baseline, increased, and non-Newtonian fluid viscosity cases, respectively.

Velocity from the 2D CFD model during the 0.5 mm/s subluxation reached a maximum of 106.8 mm/s, i.e., over 200 times that of the femoral head movement. As for the 3D situation, the maximum velocity occurred at the entrance to the gap between the femoral head and acetabular cup, at the beginning of the subluxation event. Parametric exercise of the 2D model showed that, presumably due to finite viscous drag of the fluid, there was not a singularity (instantaneous infinite velocity at the initiation of outward head movement) even for a vanishingly small ($\ll$ 0.1 mm) initial gap.

A representative velocity vector field from the EdPIV software is shown in Figure 3. The agreement between velocity magnitude of the 2D CFD model and PIV results was 85% or better for the clearly visualizable areas (1) outside the entrance to the gap and (2) farther down the gap towards the pole of the acetabular cup (Figure 9). The fluid velocity immediately at the gap entrance unfortunately was too high to be reliably measured with the PIV.

DISCUSSION

A 3D CFD model of total hip subluxation, validated by a PIV in a corresponding 2D CFD analog, was utilized to explore a mechanism through which third body debris suspended in the joint fluid might be drawn well into the bearing space during subluxation of a total hip. The results showed that there is a large fluid ingress velocity into the space between the bearing surfaces as the femoral head began to separate from the acetabular cup. It was shown that even very small subluxations (<0.6 mm) could lead to high fluid ingress velocities. Third body particles suspended in the fluid could gain access to the articulating surfaces in this manner. Pathlines were computed to determine how far third body debris suspended in the joint fluid might travel. Depending on the specifics of the hip implant design, debris originating at the maximum-velocity ingress site could reach within 11° of the pole of the acetabular cup.

When pathlines were computed all around the equator of the femoral head at the entrance to the gap between the acetabular cup and femoral head, it was revealed that there was an area in the acetabular cup that was unreachable even after 0.015 seconds into the subluxation. Unfortunately, this area was located inferomedially, relatively remote from the locations of third body particle embedment that are most problematic for wear increase (superolateral) (Lundberg et al., 2006). Pathlines also showed that suspended third body debris needed to be located relatively close to the entrance to the bearing space in order to be drawn in.

Measurements of the synovial fluid viscosity have varied by more than three orders of magnitude (Mazzucco et al., 2004). To explore the effect of fluid viscosity on fluid ingress velocity, the viscosity of synovial fluid in the CFD model was varied over six orders of magnitude. When the fluid viscosity was decreased to 0.001 Pa-s (the same viscosity as water), fluid pathlines showed that suspended third body particles would travel through about 27° less arc length than if the fluid viscosity was three to six orders of magnitude higher. Non-Newtonian fluid viscosity (based on data from 35 total knee arthroplasty patients, (Mazzucco et al., 2004)) resulted in fluid pathlines approximately equal to those for the lower fluid viscosities.

Larger femoral head diameters and smaller clearance widths both served to increase fluid velocity at all points around the entrance to the gap. Fluid velocity was greatest along the anterosuperolateral cup edge, for all head sizes and clearance widths. Fluid pathlines indicated that suspended debris would reach nominally similar angular positions on the cup with larger head sizes, despite absolute fluid velocity being greater for larger head sizes. This suggests that head diameter per se involves neither exacerbation nor attenuation of particle ingress, for otherwise similar subluxation angles. For a given neck diameter, of course, increasing head diameter increases the angular range of motion prior to impingement. So, the correspondingly lessened propensity for fluid-convected third body ingress needs to be added to the list of recognized advantages of larger head size.

The one implant design parameter that did appear to influence how far suspended third body debris could reach was head inset. A head inset of −2 mm decreased the amount of acetabular cup coverage of the femoral head by 8.2° (from 50° for 0 mm head inset to 41.8° for −2 mm head inset). The fluid velocity magnitude for the −2 mm head inset case was greatly reduced from the baseline case during subluxation, translating into less distance that could be traveled by suspended third body particles. Conversely, a +2 mm head inset resulted in greatly increased fluid velocity magnitude relative to the baseline case. Solutions for the +2 mm head inset case could only be obtained for part of the subluxation (0–0.008 seconds), but even in that abbreviated time, suspended third body debris could already be transported through essentially the same arc length as during a full 0.012 seconds for the 0 mm head inset case.

In this study, smaller head sizes, larger gap widths, and decreased femoral head inset resulted in lower fluid ingress velocity into the space between the bearing surfaces during the leg-cross subluxation. These implant characteristics could translate into decreased distance of third body particle ingress. The movement of fluid into the bearing space during a single leg-cross subluxation was investigated in this study. Additional studies could be performed to explore the fluid movement for yet additional designs, or during other subluxation activities and different combinations of subluxation activities. The final position of third-body-laden fluid would change depending on the specific subluxation activity, the number of subluxations that occurred, and the combination of subluxation events. Presumably, some subluxation activities could result in clearing of third body particles from certain locations within the bearing space, while some could result in entrapment of third body particles between the bearing surfaces. These entrapped particles could later become embedded and roughen the femoral head surface, increasing polyethylene wear.

Wear increase from third body debris ingress occurring as a result of subluxation of the hip implant is a plausible clinical consequence of impingement, even in the absence of frank dislocation or polyethylene delamination. The present results indicate that implant designs aimed at reducing subluxation of the hip implant would therefore also be beneficial in reducing third body burden clinically. Of course, reducing the problem at its source - third body debris generation - is even more desirable.

Acknowledgements

Grants from the NIH (AR46601, AR47653), DePuy, Inc., and an NSF graduate research fellowship supported this research. Technical assistance was provided by Mr. Liam Glennon and Dr. Ceyda Polatel.

References

Dowd JE, Sychterz CJ, Young AM, Engh CA. Characterization of long-term femoral-head-penetration rates. Association with and prediction of osteolysis. Journal of Bone & Joint Surgery - American Volume 2000;82:1102–1107.

Dumbleton JH, Manley MT, Edidin AA. A literature review of the association between wear rate and osteolysis in total hip arthroplasty. Journal of Arthroplasty 2002;17:649–661. [PubMed: 12168184]

Hall RM, Siney P, Unsworth A, Wroblewski BM. Prevalence of impingement in explanted charnley acetabular components. Journal of Orthopaedic Science 1998;3:204–208. [PubMed: 9662663]

Jasty M, Goetz DD, Bragdon CR, Lee KR, Hanson AE, Elder JR, Harris WH. Wear of polyethylene acetabular components in total hip arthroplasty. An analysis of one hundred and twenty-eight components retrieved at autopsy or revision operations. Journal of Bone & Joint Surgery - American Volume 1997;79:349–358.

Komistek RD, Dennis DA, Ochoa JA, Haas BD, Hammill C. In vivo comparison of hip separation after metal-on-metal or metal-on-polyethylene total hip arthroplasty. Journal of Bone & Joint Surgery - American Volume 2002;84:1836–1841.

Lombardi AV Jr, Mallory TH, Dennis DA, Komistek RD, Fada RA, Northcut EJ. An in vivo determination of total hip arthroplasty pistoning during activity. Journal of Arthroplasty 2000;15:702–709. [PubMed: 11021445]

Lundberg HJ, Stewart KJ, Pedersen DR, Callaghan JJ, Brown TD. Problematic sites of third body embedment in polyethylene for total hip wear acceleration. Journal of Biomechanics 2006;39:1208–1216. [PubMed: 15894322]

Mazzucco D, Scott R, Spector M. Composition of joint fluid in patients undergoing total knee replacement and revision arthroplasty: Correlation with flow properties. Biomaterials 2004;25:4433–4445. [PubMed: 15046934]

Nadzadi ME, Pedersen DR, Callaghan JJ, Brown TD. Effects of acetabular component orientation on dislocation propensity for small-head-size total hip arthroplasty. Clinical Biomechanics 2002;17:32–40. [PubMed: 11779644]

Shon WY, Baldini T, Peterson MG, Wright TM, Salvati EA. Impingement in total hip arthroplasty - a study of retrieved acetabular components. Journal of Arthroplasty 2005;20:427–435. [PubMed: 16124957]

Stewart KJ, Pedersen DR, Callaghan JJ, Brown TD. Implementing capsule representation in a total hip dislocation finite element model. Iowa Orthopaedic Journal 2004;24:1–8. [PubMed: 15296198]

Yamaguchi M, Akisue T, Bauer TW, Hashimoto Y. The spatial location of impingement in total hip arthroplasty. Journal of Arthroplasty 2000;15:305–313. [PubMed: 10794226]

Yamaguchi M, Hashimoto Y, Akisue T, Bauer TW. Polyethylene wear vector in vivo: A three-dimensional analysis using retrieved acetabular components and radiographs. Journal of Orthopaedic Research 1999;17:695–702. [PubMed: 10569478]

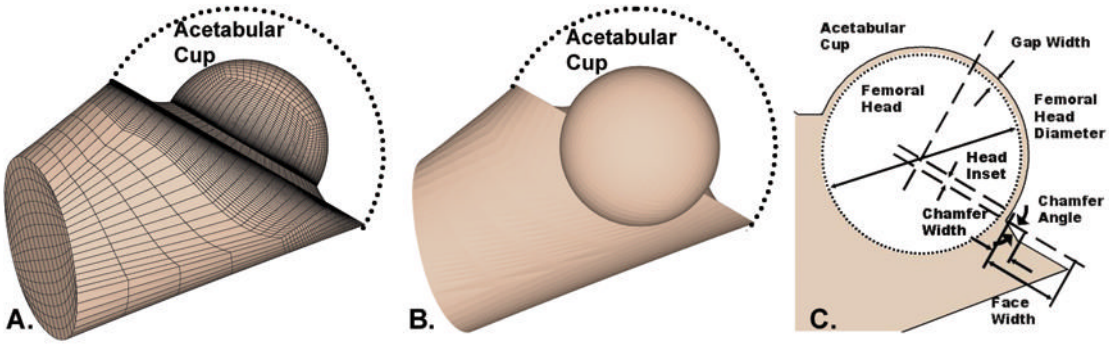

Figure 1.

3D CFD model of leg-cross subluxation. A. Outer model view with visible mesh. The mesh shown is the capsule-enclosed region of the joint space. B. Transparent view of the model with visible femoral head surface. (The femoral component neck was not included in the model.) C. Schematic showing the variables parametrically studied using the 3D CFD model of leg-cross subluxation. Note that chamfer width is defined in terms of percentage of the acetabular face width (thickness of the polyethylene liner).

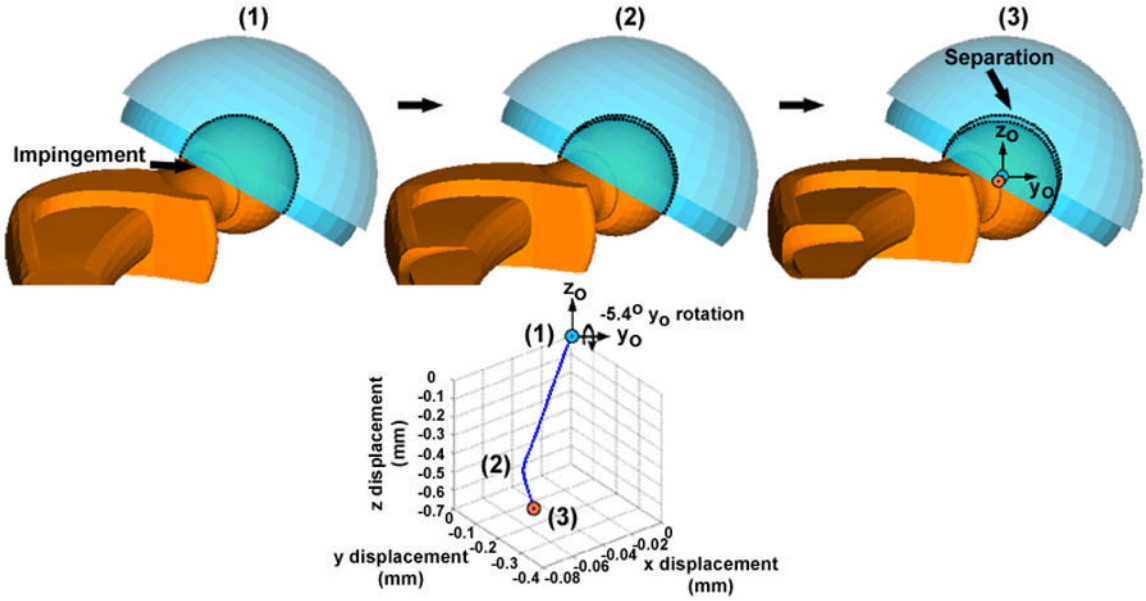

Figure 2.

Three successive solution steps from the FE model of THA dislocation (Nadzadi et al., 2002). Steps shown are from impingement initiation (1) to ~1.24 mm of total subluxation/ separation (3) between the femoral head and acetabular cup. The line shows the kinematics of the femoral head center applied to the CFD model during the subluxation.

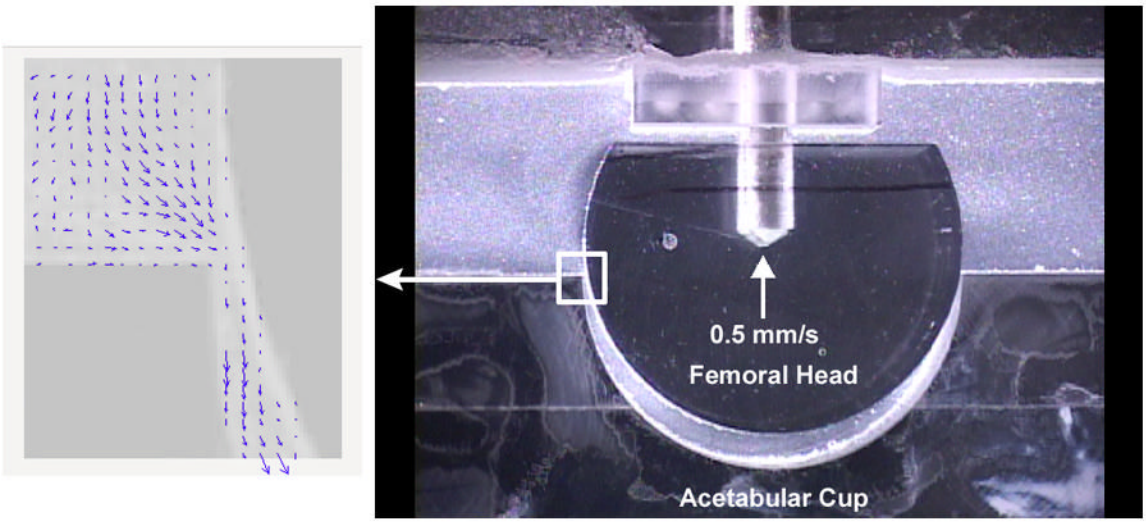

Figure 3.
Example image taken during PIV analysis of the femoral head upward subluxation (right). Note the white tracer particles in the fluid. Representative output image from EdPIV (left), showing fluid velocity vectors for the 0.5 mm/s of vertical subluxation.

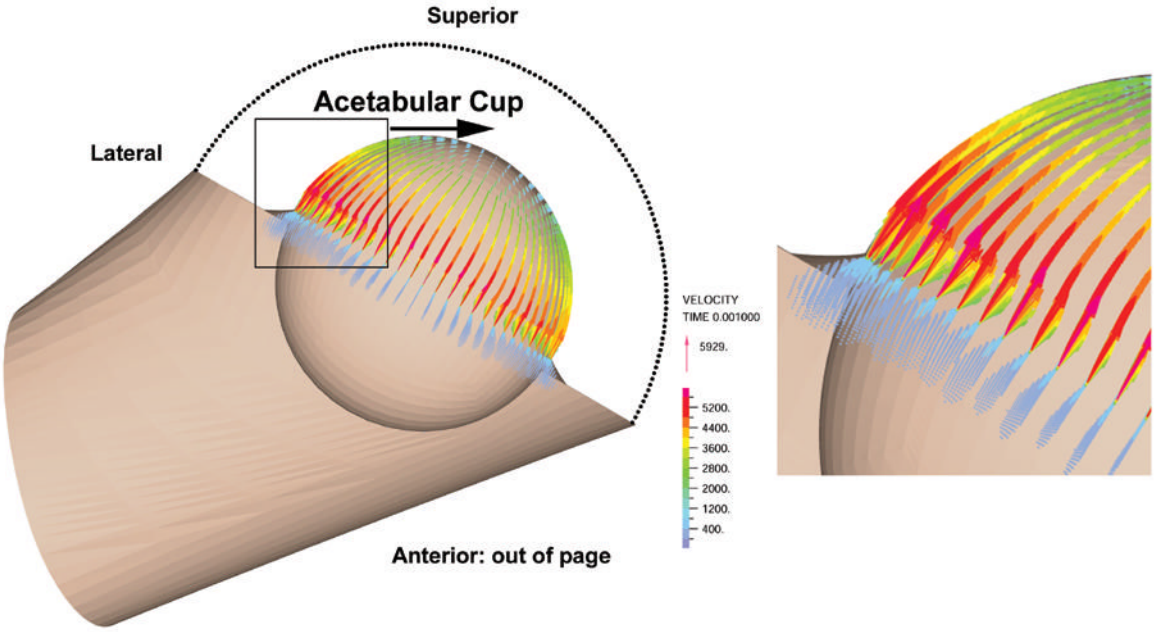

Figure 4.
Fluid velocity vectors at the first time-step (time = 0.001 seconds) for the 3D CFD model of leg-cross subluxation. As indicated by the vectors pointing into the gap between the femoral head and acetabular cup, fluid moves into the cup at high velocity at the initiation of subluxation.

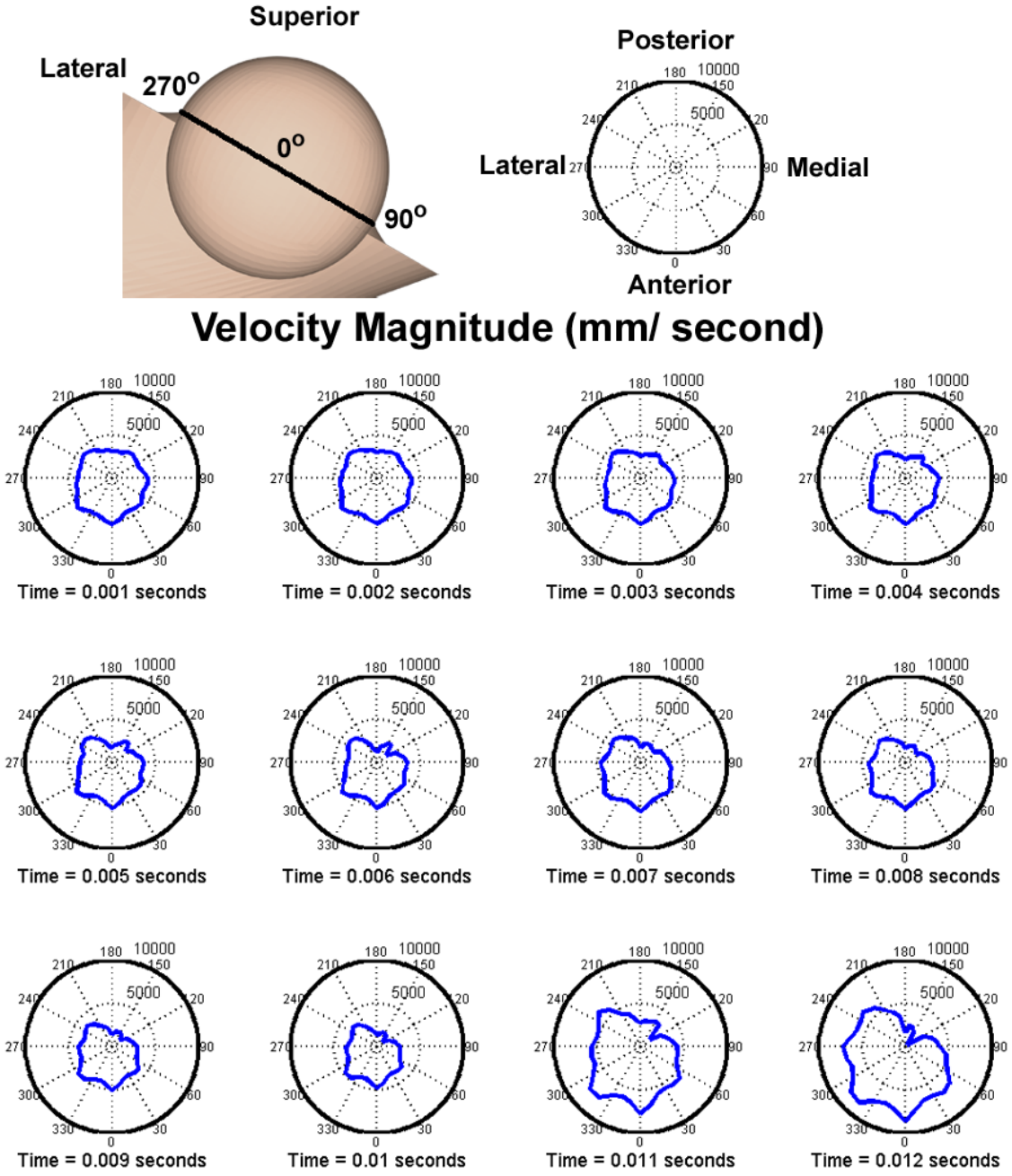

Figure 5.
Fluid velocity magnitude (mm/second) progression for each time-step of the 3D CFD model of leg-cross subluxation. Velocity magnitude is shown at a circumferential line around the equator of the femoral head, where 0° is in the anterior direction and 270° is the lateral-most point of the acetabular cup.

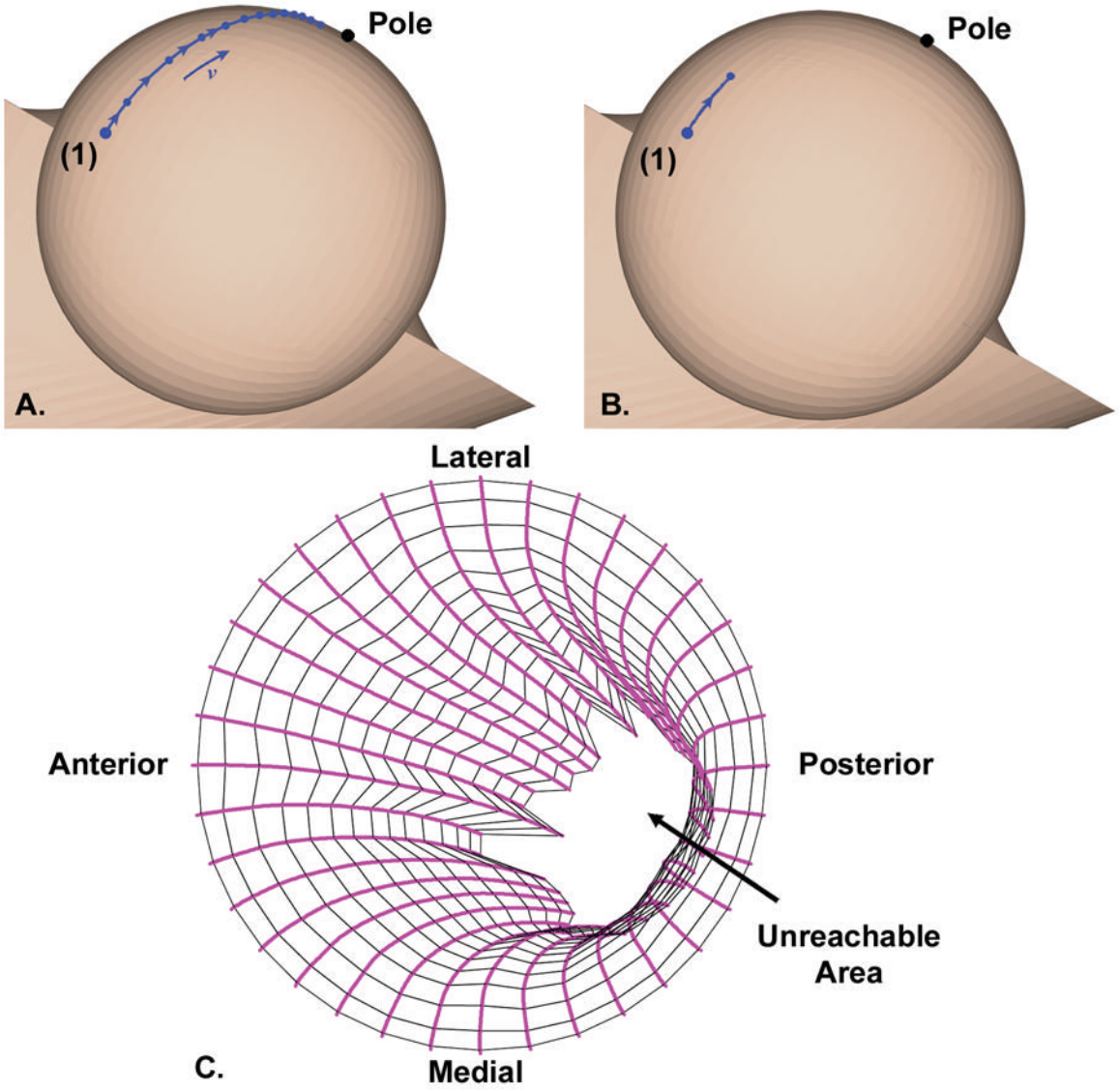

Figure 6.

A. and B. Pathline for fluid beginning at location (1) and time 0.000 seconds (A), or at time 0.011 seconds (B) during the leg-cross subluxation. Each dot along the pathline indicates the position of the fluid for successive time points, in 0.001-second increments, up to the end of the subluxation (0.012 seconds). C. Enface view of the acetabular cup, with pathlines showing the area potentially reachable by third bodies during the subluxation. The pathlines start from the equator of the femoral head. Lines connecting each pathline show the pathline endpoints for successive timepoints from 0.000 to 0.015 seconds.

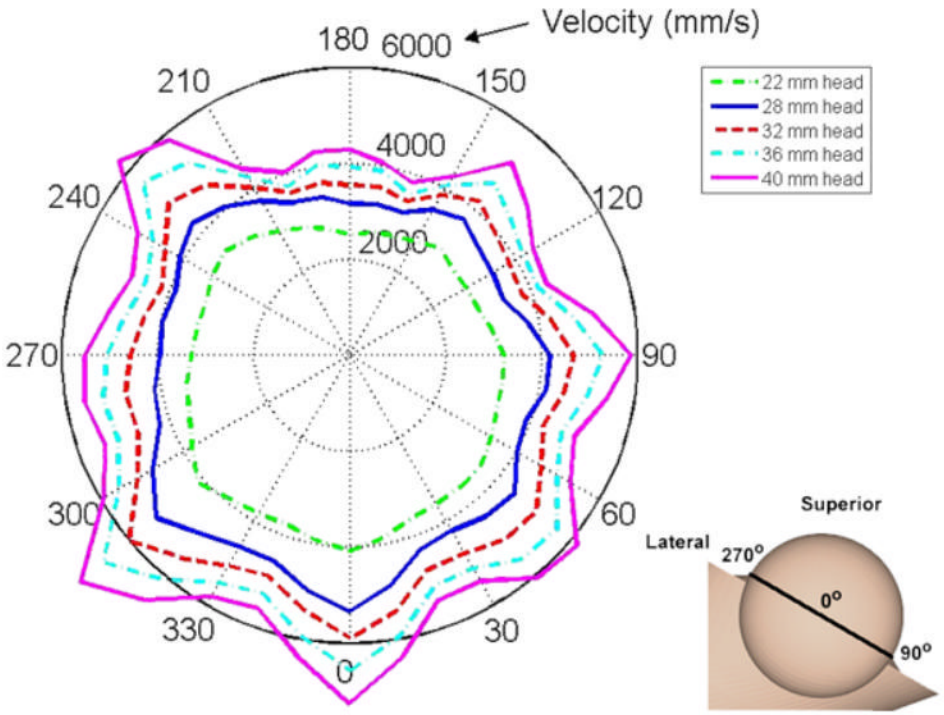

Figure 7.
Fluid ingress velocity magnitude (time=0.001 seconds) for the 3D CFD model of leg-cross subluxation, for five different femoral head diameters. Velocity magnitude is shown at a circumferential line around the equator of the femoral head, where 0° designates the anterior direction and 270° is the lateral-most point of the acetabular cup.

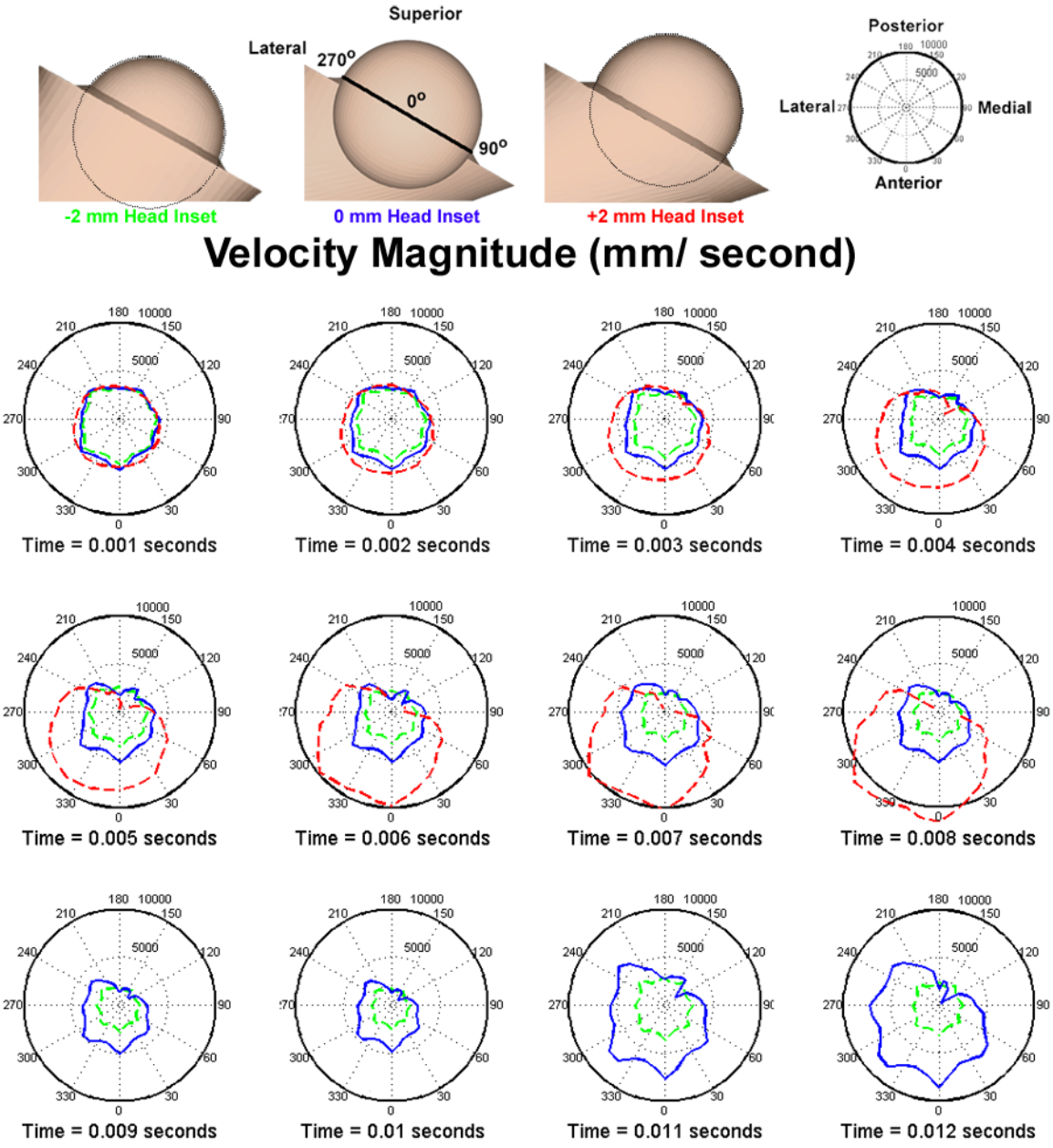

Figure 8.
Progression of fluid ingress velocity magnitude for the 3D CFD model of leg-cross subluxation for three different head inset values.

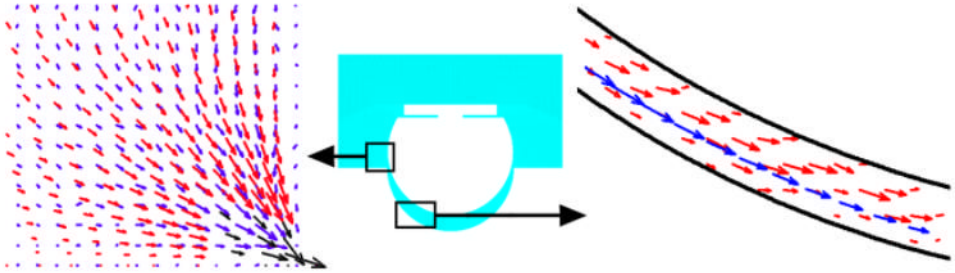

Figure 9.
Fluid velocity vectors for PIV (blue vectors) vs. 2D CFD (red and black vectors). The red CFD vectors are scaled so that the same length vectors for PIV (blue) have equal magnitudes. The black CFD vectors are scaled so that blue PIV vectors of the same length are %50 less in magnitude.

Table 1

Kinematics output from the FE model. Figure 2 shows the origin and directions for the x-y-z coordinate system. Note that x-, y-, and z- displacement refers to the change in position of the center of the femoral head starting from (x_o, y_o, z_o) at (0, 0, 0), or step 0 in this table.

Step	x-displacement (mm)	y-displacement (mm)	z-displacement (mm)	y-rotation (radians)	Total Separation (mm)
0	0	0	0	0	0
1	−0.0625	−0.192	−0.389	−0.079	0.438
2	−0.0790	−0.549	−1.106	−0.157	1.237

Table 2

Variables parametrically studied with the 3D CFD model of leg-cross subluxation.

	Femoral Head Diameter (mm)	Gap Width (mm)	Chamfer Angle (°)	Chamfer Thickness (% of Polyethylene Liner Thickness)	Head Inset (mm)	Fluid Viscosity (Pa s)
Baseline	**28**	**0.1**	**30**	**25**	**0**	**1**
1	22 32 36 40	Baseline	Baseline	Baseline	Baseline	Baseline
2	Baseline	0.05 0.20	Baseline	Baseline	Baseline	Baseline
3	Baseline	Baseline	0 60	Baseline	Baseline	Baseline
4	Baseline	Baseline	Baseline	10 40	Baseline	Baseline
5	Baseline	Baseline	Baseline	Baseline	−2 2	Baseline
6	Baseline	Baseline	Baseline	Baseline	Baseline	0.001 1000 Non-Newtorian